Experimental evidence of chloride induced trap passivation in lead halide perovskites through single particle blinking studies

Handong Jin, Julian A. Steele, Ruolin Cheng, Nagma Parveen, Maarten B. J. Roeffaers, Johan Hofkens and Elke Debroye**

Dr. H. Jin, Dr. R. Cheng, Dr. N. Parveen, Prof. J. Hofkens, Dr. E. Debroye
Department of Chemistry, KU Leuven, Celestijnenlaan 200F, Leuven, Belgium
E-mail: johan.hofkens@kuleuven.be; elke.debroye@kuleuven.be

Prof. J. Hofkens
Max Planck Institute for Polymer Research, Ackermannweg 10, 55128 Mainz (Germany)

Dr. J. A. Steele, Prof. M.B.J. Roeffaers
Centre for Membrane Separations, Adsorption, Catalysis and Spectroscopy for Sustainable Solutions (cMACS), KU Leuven, Celestijnenlaan 200F, Leuven, Belgium

Keywords: Lead halide perovskites, photoluminescence blinking, defects, charge carrier traps, trap passivation

Research into organic-inorganic lead halide perovskites as photoactive material in solar cells and other electro-optical devices has made immense progress in recent years. However, efficiency losses resulting from deep traps associated with framework defects, still limits the performance of perovskite semiconductors. Defect passivation by the incorporation of dopants, such as chloride doping in methylammonium lead iodide ($MAPbI_3$) perovskite, is stated as one of the most efficient ways to reduce trap densities. Commonly used parameters like improved photoluminescence (PL) quantum yields and extended PL lifetimes provide non-conclusive experimental evidence on trap density suppression by chloride doping. In this work, the effect of chloride doping on the crystal morphology, composition, and PL of $MAPbI_3$ nanocrystals (NCs) was carefully investigated. Besides the anticipated enhanced PL intensity and extended PL lifetime, single-particle PL intermittency studies revealed brighter and longer ON-states with increasing amounts of chloride doping, which represents additional evidence of effective chloride-induced trap passivation. These findings provide important guidelines for generating lead halide perovskite materials with significantly reduced trap densities towards the fabrication of high-performance optoelectronic devices.

1. INTRODUCTION

Organic-inorganic metal halide perovskites (OMHP) are very promising semiconductor materials for optoelectronic devices.[1] Their intense light absorption, low exciton binding energy, long charge carrier lifetime and diffusion lengths make these materials great candidates for photovoltaic (PV) applications. In a decade, the power conversion efficiency of perovskite solar cells (PSCs) has swiftly climbed from 3.8% in 2009[2] to 25.2%.[3] However, poor long term stability and high defect densities are still the two issues hindering PSC commercialization.[4] Compared to the defect densities of traditional semiconductors, such as, Si (~10^{8} cm^{-3}), CdTe (10^{13}-10^{16} cm^{-3}), CIGS (Cupper Indium Gallium Selenide 10^{11}-10^{15} cm^{-3}), GaN (~5×10^{15} cm^{-3}) and GaAs (10^{13}-10^{15} cm^{-3}), solution-processed polycrystalline OMHPs exhibit slightly higher defect densities (10^{16}-10^{17} cm^{-3}), however, monocrystalline perovskites exhibit a significantly improved structural quality and subsequent lower amount of densities (10^{9}-10^{11} cm^{-3}).[5] Although the majority of structural defects, with energies just above or below the conduction band and valence band, are known not to cause carrier trapping, the main action point for improving PSC performance is controlling harmful defect-associated charge carrier traps with energies within the bandgap. These traps result in efficiency losses by non-radiative recombination.[5-6]

Despite the use of sophisticated synthetic techniques and strictly controlled reaction conditions, the formation of harmful native defects during OMHP crystal growth cannot be avoided[5, 7]. For example, $MAPbI_3$ exhibits high trap densities in both polycrystalline (10^{16}-$10^{21}cm^{-3}$) and single crystalline ($10^{10}cm^{-3}$) morphologies.[5] Still, $MAPbI_3$ is the most popular material explored for PSCs due to its suitable bandgap (~1.5 eV) compared to its chloride and bromide counterparts.[8] Much attention has been paid to investigate and mitigate the harmful defects, such as interstitials,[8] in $MAPbI_3$ perovskites. So far, Density Function and First Principle

calculations are the most powerful and direct tools for exploring the origin of traps and predicting possible solutions to decrease trap densities.[8-9] For example, in lead iodide perovskite materials, iodide interstitials are regarded as potential deep traps by First Principle calculations, and it has been reported that bromine and chlorine doping can effectively neutralize these iodine traps.[8] Although iodide vacancies have been established as non-harmful defects with their energy level close to the conduction band,[5] Nan *et al.* claimed[10] that chloride doping can suppress the formation of discrete traps related to iodide vacancies. Because of the weak Pb-I bond and easy iodide ion migration, iodide vacancies are readily formed behaving similar to a lead interstitial.[10] Moreover, Cl^- at grain boundaries in OMHP thin films also effectively passivates surface defects, enhancing PL intensity.[11] Thus, chloride doping is beneficial for reducing both intrinsic (vacancies, interstitial, antisites, ….) and extrinsic defects (surface defects, grain boundaries, ...). Unfortunately, conclusive experimental evidence on chloride-induced trap passivation has not yet been provided.

The commonly employed optical parameters to assess the impact of traps on the OMHP performance include PL quantum yield (PLQY) and PL lifetimes. However, traditional PL enhancement and longer PL lifetimes may not be conclusive for trap density suppression, since the improvement of these parameters can be related to potential morphology changes, rather than effective defect passivation. For example, generally, grain boundaries (GBs) refer to the interface between two grains in polycrystalline materials and are 2D defects in the crystal structure, decreasing the electrical and thermal conductivity of the materials. The detection of longer PL lifetimes can be be attributed to the formation of less grain boundaries (GBs), while trap densities in the grains remains the same. Saidaminov *et al.* reported a substantial PL enhancement, longer PL lifetime, and an improved PV efficiency for Cl^- doped $Cs_{0.05}MA_{0.15}FA_{0.8}PbI_{2.55}Br_{0.45,}$[12] yet at the cost of material stability. Likewise, Hwang *et al.* found that Cl^- passivation of $MAPbI_3$ thin films resulted in an enhanced PL intensity and an

extended PL lifetime, however, with inferior PV efficiency compared to the pristine perovskite.[13] In contrast, the same research group found an improved PV performance for Cl^- post-treated $(Cs_{0.05}FA_{0.79}MA_{0.16})Pb(I_{0.84}Br_{0.16})_3$ perovskite films but with a decreased PL intensity and shorter PL lifetime.[13] Hence, more direct and advanced optical techniques to quantify trap densities are required.

Studying PL blinking behavior in OMHP single particle has emerged as a reliable method to unravel charge carrier dynamics in light-emitting materials.[14] PL intermittency (blinking) is the temporal PL intensity fluctuation assigned to a photo-assisted switching between a bright, neutral state (weak or no quenching = "ON" state) and a dim, charged state (strong luminescence quenching = "OFF" state). Several mechanisms have been proposed to describe the blinking behavior in OMHP particles. It is generally accepted that PL blinking is attributed to the switching between an active and passive state of non-radiative or deep trap recombination centers.[15] Trap density variations or ion migration[16], greatly affecting carrier dynamics, can be revealed by analyzing PL blinking data of individual OMHP particles, which are hard to probe using normal optical techniques such as steady-state PL and time-resolved PL.

Generally, monocrystalline OMHP nanocrystals exhibit relatively low trap densities,[5, 15, 17] and the charge carrier dynamics affecting the optical and electronic properties can be systematically and independently probed because of the absence of grain boundaries. In this paper, we examine the effect of chloride doping in $MAPbI_3$ NCs on the NC morphology, crystalline quality, and the bulk as well as single particle level PL properties. From these observations, the role of Cl^- in the growth and photophysical performance of $MAPbI_3$ NCs was determined. With Cl^- incorporation, the bulk PLQY increased and the PL lifetime of individual $MAPbI_3$ NCs was found to be much longer. Additionally, less blinking was observed as indicated by the more bright and longer duration of ON states (i.e. increased power-law exponents for the ON

distribution). All these experimental factors indicate lower trap densities compared with pure $MAPbI_3$ NCs.

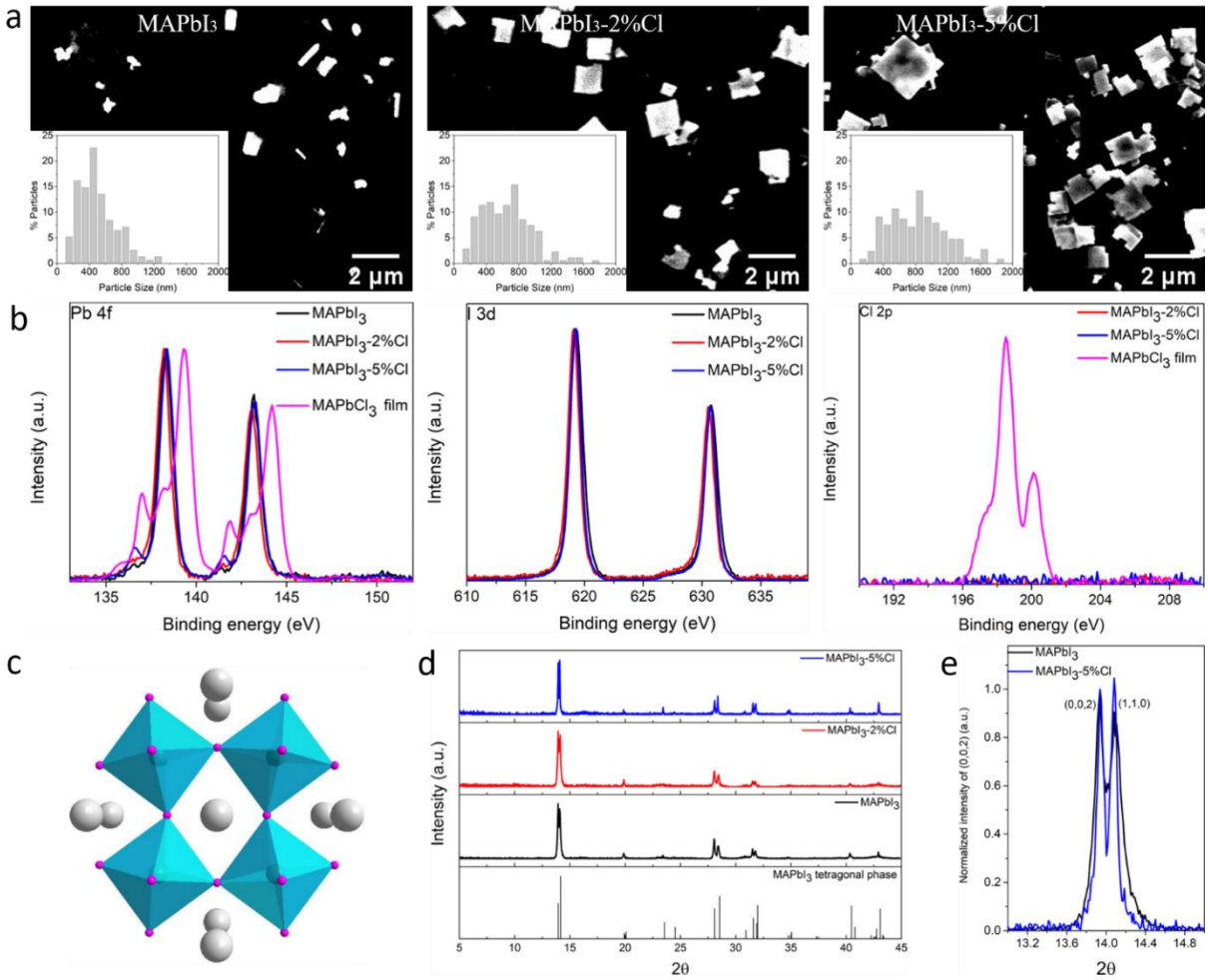

Figure 1. (a) SEM images and size distribution histogram of the edge lengths of $MAPbI_3$ nanocrystals with 0%, 2% and 5% Cl doping (dropcasting of a diluted suspension on glass slide). (b) XPS spectra of Pb 4f, I 3d and Cl 2p core levels recorded with excitation energy of 4000 eV for $MAPbI_3$ nanocrystals without and with chloride doping (dropcasted films on silicon substrate). (c) Schematic representation of the $MAPbI_3$ tetragonal phase. The grey, black and pink spheres represent MA cation, Pb, and I elements, respectively. (e) XRD patterns and (d) Comparison of (002) and (110) Bragg peaks (dropcasted films on Mylar substrate).

2. RESULTS AND DISCUSSION

2.1 Morphology, structure, and composition of $MAPbI_3$ NCs.

For pinpointing representative amounts of Cl doping to perform a reliable comparative study with pure $MAPbI_3$ NCs, six samples with different Cl content were screened, i.e. NC samples resulting from 0, 1, 2, 5, 9 and 11 molar% Cl-containing precursor solutions. According to SEM imaging (Figure 1a), for the pure $MAPbI_3$ NC sample, a mix of $MAPbI_3$ nanoplates and nanorods with an average size of 300 nanometers is observed. Based on AFM (Figure S6b), a particle thickness of 70 nm was identified. Upon chloride doping, less nanorods but more and larger nanoplates were formed, the latter with a size distribution peaking at approximately 800 nm. That means that the two doped samples contain particles with sizes of roughly the same order of magnitude as compared to the pure $MAPbI_3$ NCs. As reported previously, a templated self-assembly process via the formation of a $MAPbCl_3$ intermediate phase guides nucleation and growth in the chloride-containing systems, resulting in larger crystals.[18] With 9% and 11% Cl doping, however, the formation of nanofiber-like crystals is observed (Figure S2). This morphology change can be explained by the preferred expression of certain crystal facets due to the additional MACl in DMSO solution,[18-19] or more specifically, due to the presence of DMSO. A PL blue shift was observed for these two "heavy" Cl-doped $MAPbI_3$ NCs, while the $MAPbI_3$-1, 2 and 5%Cl samples exhibited a slight gradual red-shift (Figure S4). A similar trend was described in work by Nan *et al.*[10] in which they report that the doping procedure with a higher Cl content has a detrimental effect on the crystalline quality.[20] In order to correctly assess the changes in structure and optical properties with and without chloride doping, it is important to also consider the effect of the polar solvent DMSO, used for dissolving MACl. We established that the effect of DMSO on the crystal quality of the perovskite is minimal for the low doping levels (up to 5%Cl, see supporting information). Therefore, based on these initial screening results, further studies were selectively performed on the $MAPbI_3$, $MAPbI_3$-2%Cl, and $MAPbI_3$-5%Cl NCs (which did show very little morphology and optical changes), for obtaining a quantitative comparative study on the intrinsic variation of the structural and photophysical properties upon Cl-doping.

XPS was performed to get information on the elemental composition of the NC surface after adding chloride. Figure 1b shows the Pb 4f, I 3d and Cl 2p spectra of $MAPbI_3$, $MAPbI_3$-2%Cl and $MAPbI_3$-5%Cl. For Pb 4f, the two main peaks are attributed to Pb $4f_{5/2}$ (141-146 eV) and Pb $4f_{7/2}$ (136-140 eV), respectively. The small peak around 137 eV results from the presence of Pb^0.[21] The minor shifts in the Pb 4f spectrum fall within the region of the instrumental error (around 0.1 eV).[22] Overall, the XPS spectra of the Cl-doped samples overlap with the one of the pure $MAPbI_3$, indicating that the doping did not alter the overall electronic structure. Considering Cl 2p, no significant signal of Cl could be detected for the Cl-doped NCs. Furthermore, EDS measurements indicate a homogeneous distribution of carbon, lead, and iodide in element mapping, but did not indicate the presence of chloride, as shown in Figures S6a and c. These data suggest that the content of chloride is below the detection limits of XPS (0.1%-1%, detection depth: ~ 10 nm) and EDS (0.1%, detection depth: ~1 μm). Note that the total amount of Cl which was added to the precursor solution (2% and 5%, respectively), did not necessarily all react to be incorporated into the $MAPbI_3$ NCs. A similar observation was found in $MAPbI_3$ thin films 'heavily' doped with chloride[18, 23] in which chloride-related signals were also absent in their XPS or EDS data. A similar result for chloride doping in $FAPbI_3$ materials has also been reported in literature.[11, 24] Finally, the presence of chloride was confirmed previously by more sensitive techniques such as nano-probe X-ray fluorescence[23b] and X-ray absorption near edge structure refinement[25]. In the corresponding XRD patterns (Figure 1d), no clear peak shift can be observed for all three $MAPbI_3$, $MAPbI_3$-2%Cl and $MAPbI_3$-5%Cl samples, suggesting the same crystal structure and lattice parameters. The peaks at about $2\theta = 13.9^\circ$ and 14.1° are typically assigned to the tetragonal phase. With an increasing amount of chloride, those two peaks exhibit relative narrowing, as magnified in Figure 1e. A possible explanation is an improvement of the crystalline quality resulting from Cl doping. These results are consistent with the information obtained from DFT calculations[10] by Nan *et*

al. which predicted that the local geometric distortions can be suppressed by low chloride concentrations.

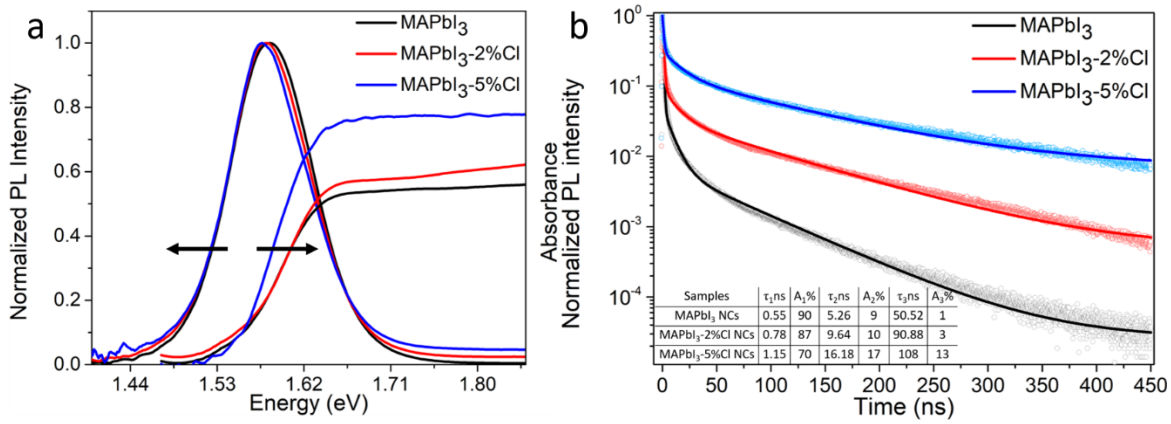

Figure 2. (a) Absorption (right) and normalized PL (left, 488 nm excitation) spectra of $MAPbI_3$ NCs with 0%, 2% and 5%Cl. (dropcasted film on a quartz substrate) (b) Normalized time-resolved PL decay and fitted curves for $MAPbI_3$-0, 2 and 5%Cl NCs (drop of NC suspension on a cover glass), measured in air with pulsed excitation (485 nm, 2 MHz, 4.85×10^{12} photons/cm^2). The inset table displays the extracted fitting parameters, i.e. three lifetime components and corresponding amplitudes for each set of NCs.

2.2 PL, PL lifetime, and PL blinking behavior of $MAPbI_3$ NCs in air.

Figure 2a depicts the absorption and normalized steady-state PL spectra. With increasing Cl content, a small but clear redshift in PL (about 10 meV) and absorption (~10 meV) can be observed, which supports the notion of improved crystallinity within the Cl-doped $MAPbI_3$ NCs. The pure $MAPbI_3$ NCs exhibit a PL quantum yield (PLQY) of 7.5% (Excitation power density 0.9 mW/cm^2). This value is relatively low when compared to literature,[26] where they report PLQY values of 20-30% for $MAPbI_3$ NCs of roughly 20 nm. However, the crystals studied here are more than an order of magnitude larger, and size effects comes into play. Upon incorporation of 5% of chloride, the value reached 13% (same excitation power density as for undoped sample), which is almost two times the value obtained for pure $MAPbI_3$ NCs. The average lifetimes of $MAPbI_3$, $MAPbI_3$-2%Cl and $MAPbI_3$-5%Cl NCs were measured, as these strongly correlate to the charge diffusion dynamics and recorded power conversion efficiency

(PCE) of perovskite solar cells. Normally, intrinsic recombination is considered when studying carrier lifetimes. In reality, PL decay time is related to many factors such as crystal size and shape,[27] defect type, and defect density.[28] Obviously, for deep traps, in which non-radiative recombination takes place, lower trap densities favor longer lifetimes. The trapping and trap-escaping time strongly depend on the trap types and location of surface defects.[5] In order to gain more information on these emission dynamics, the fluorescence decay of an ensemble of NCs deposited on glass cover slides was measured by using time correlated single photon counting (TCSPC, Figure 2b). Lifetime information has been be extracted by fitting the decay curves; the fitting parameters of the $MAPbI_3$ NCs with different contents of chloride are shown in the inset of Figure 2b. The $MAPbI_3$ NCs show lifetime τ values of 0.55 ns (τ_1), 5.26 (τ_2) and 50.52 ns (τ_3), respectively. In general, the decay curves show that the PL lifetime increases substantially with the chloride content. Upon 5% chloride doping, the shorter decay times τ_1 and τ_2 are tripled for the crystals with 5% doping, while the contribution of τ_1 substantially decreased in favor of the long component. In fact, a τ_3 value of 108 ns is measured, which is almost double the one of pure $MAPbI_3$ NCs, and which exhibits a significantly higher contribution (A_3 = 13% VS 1%, respectively). A similar phenomenon was reported by Son *et al.*[29] and Jung *et al.*[30] for passivated $MAPbI_3$ by MAI and octylammonium iodide, respectively. Except for an increased average lifetime after passivation, they reported that a higher contribution of the longer lifetime results from a larger number of free charge carriers, indicating a strongly suppressed trap-assisted recombination.[29] Actually, the lifetime components can be assigned to different physical origins. [31] The shorter component has been related to the radiative recombination at the NC surface states and the intermediate lifetime has been attributed to exciton recombination.[31] The longer lifetime component is attributed to free charge carrier propagating deeper in the materials. The overall observed longer lifetimes thus point towards reduced trap-assisted non-radiative recombination to bulk and/or surface states, thereby increasing the diffusion length of photo-generated electrons and holes.

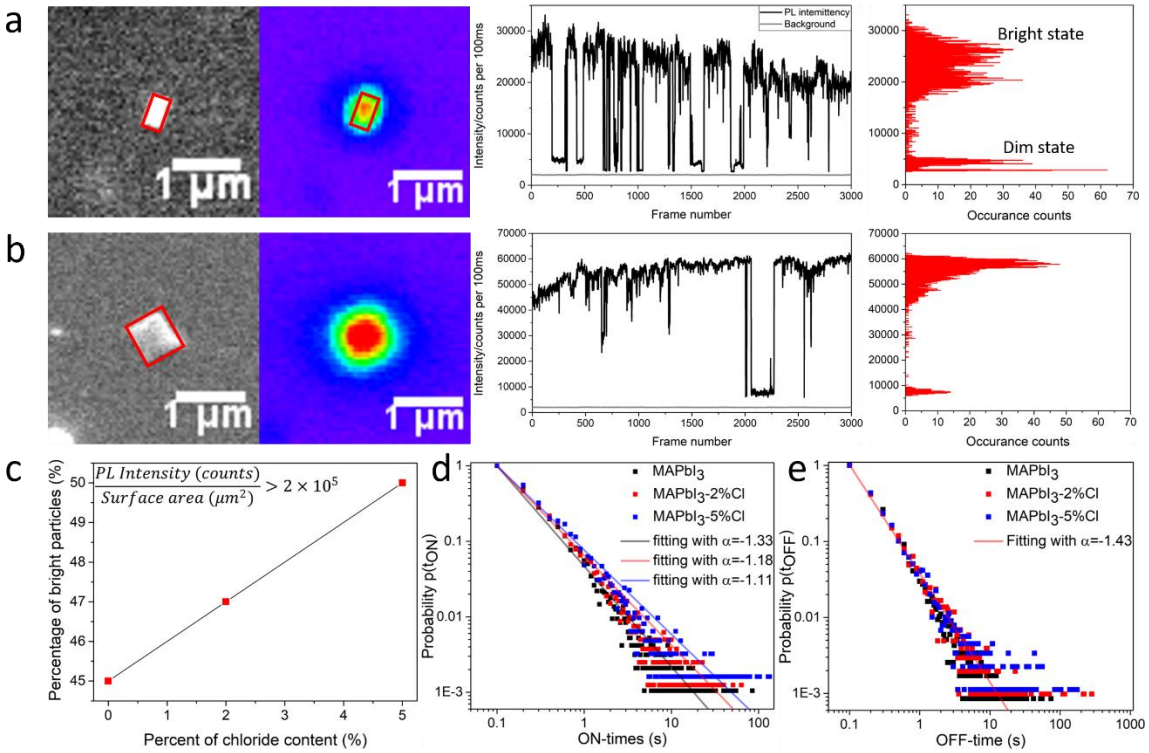

Figure 3. (a) SEM image (left), and corresponding PL image, PL time trace (right to the central) of the same NC and its corresponding histogram (right) of PL intensity of a single $MAPbI_3$ (b) and $MAPbI_3$-5%Cl (b) NC, with the examination area shown by the red square. (c) Proportion of bright single particles (PL intensity (counts)/surface area (μm^2) > 2 x 10^5) with incorporation of 0%, 2%, and 5% Cl. Normalized probability distributions of the duration of (d) ON times and (e) OFF times of $MAPbI_3$ NCs with 0%, 2% and 5% Cl doping. (over 40 individual NCs for each of the $MAPbI_3$, $MAPbI_3$-2%Cl, and $MAPbI_3$-5%Cl samples. The ON/OFF events of $MAPbI_3$ NCs with 0%, 2% and 5%Cl are 2977/2976, 2752/2749, and 2445/2453, respectively.)

When performing PL blinking experiments, it is important to only consider the PL intermittency of individual, non-clustered NCs[17] in order to correctly quantify the potential change of trap densities without and with chloride doping by excluding grain boundaries. This is made possible by correlated wide-field microscopy/SEM imaging.[32] (Figures S8) For a detailed explanation on recognizing biased data sets, please consult the SI, Figures S9-S12. Most importantly, the PL blinking behavior of single NCs located in or near a nanocluster does not represent intrinsic conditions and should not be considered.

Hence, only individual NCs were selected for monitoring the PL intensity intermittency. When collecting PL intensity transients of a single $MAPbI_3$ NC within a field of view of 32 µm x 32

μm, well-defined bright (ON) and dim (OFF) states can be observed (Figure 3a). The intensity of the OFF state is much higher than that of the background, offering solid data sets for doing reliable analysis. Besides the conventional PL blinking with binary behavior (ON and OFF state), the intermittency in some NCs shows multiple discrete PL levels (Figure S14) indicating a variation of trap densities in single NCs with time. Indeed, the impact of a defect can vary depending on time, light irradiation, environmental condition, or one defect type can transform to another by electronic excitation and/or reaction with another defect. These trap dynamics are often assigned to ion migration.[6] In these experiments, a gradual decrease in PL intensity upon illumination can be observed. A comparable PL decrease has been reported for $MAPbI_3$ microcrystals[33] and $CsPbI_3$ QDs[34] and may arise from perovskite degradation.[34-35] Notably, with the incorporation of chlorine (Figure 3b), a larger amount of bright particles could be observed with longer "ON" times. It is noted that the gradual PL decrease is not present for Cl-doped NCs, at least not in the time window for collecting the PL intensity transient, pointing at increased stability toward light-induced perovskite degradation. Moreover, the PL brightness increased with the Cl content (Figure 3c), conform the higher PLQY values as discussed before. The distribution of the average brightness is depicted in Figure S15. Figures 3d and 3e show the histograms of the duration of ON and OFF times of blinking events recorded on over 40 individual NCs of each the $MAPbI_3$, $MAPbI_3$-2%Cl, and $MAPbI_3$-5%Cl samples. Each time trace was recorded for 300 s at the same laser power density of 50 mW/cm^2. Generally, the observation of the power-law behavior of ON/OFF-state for single emitters is related with the exponential distribution of the spatial locations and energies of the trap(s) present in/near the emitter.[36] This power-law distribution, applied to single emitters, can be expressed by the probability formula comprising the time spent in the ON and OFF state, respectively, $p(t_{OFF}/t_{ON}) \propto t^{\alpha}$.[36] Even though the choice of a threshold value to determine the PL trajectories into ON and OFF can greatly affect the probability distribution,[37] the variations between the distributions containing several thousands of events each, comprise a reliable and established

procedure to monitor trap density changes. The power-law exponents α used for fitting t_{ON} and t_{OFF} for the pure and Cl-doped NCs are given in Figures 3e and 3f. (Figure S16) Interestingly, almost the same exponent α was applied for fitting the OFF distribution, which may arise from similar active rates of charge trapping. The ON state was found to appear more frequent and last longer with an increasing amount of chloride doping. Upon increasing the content of chloride, the average ON time increased as well, from 1.29 s to 3.10 s. The ON distributions hence exhibit slightly higher power-law exponents, ranging from α=-1.33 to -1.11 for pure $MAPbI_3$ and $MAPbI_3$-5%Cl NCs, respectively. The power-law distributions of ON and OFF times are directly related to the rates of switching between passive and active states of the deep trap-assisted non-radiative recombination centers. In line with the increased brightness of the chloride-doped NCs, the higher α exponents for the ON distribution indicate a more stable passive state after adding Cl, even though the chloride content is very small. Actually, DFT calculations and some experimental efforts have been carried out on exploring the nature and effect of chloride dopants. Based on DFT, suppressed lattice distortions and defect densities can be achieved.[10] As a confirmation, the defect activation energies for $MAPbI_3$ and $MAPbI_{3-x}Cl_x$ vary from a relatively deep (74.4 meV) to a shallow level (21.6 meV) revealed by capacitance-voltage measurement.[38] Similarly, longer diffusion lengths of over 1 μm for $MAPbI_{3-x}Cl_x$ compared to pure $MAPbI_3$ (100 nm) were reported by Chen *et al.*[7b] Moreover, Tan *et al.*[39] have shown chloride can act as an effective passivation agent at the interface of perovskite and TiO_2 layers due to the much higher formation energy of Pb-Cl anti-site defects (shallow) in comparison to that of Pb-I anti-site defects (deep). However, until now, no systematic effort to connect these simulations with experiments has been reported. Complementary to the prolonged lifetimes observed for Cl-doped $MAPbI_3$ NCs, the increase of power-law exponents in this PL blinking study appropriately quantifies the decrease of trap densities, building the bridge between DFT predictions and experimental results on chloride doping.

2.3 Comprehensive analysis of blinking statistics.

To explain the power-law behavior of ON and OFF distributions of QDs, several blinking models have been proposed.[36, 40] However, recent work has revealed that the blinking in OMHP nano- and microcrystals is actually mechanistically different from blinking in quantum dots (QDs).[15, 41] For example, Auger-induced non-radiative recombination does not contribute to the blinking in large OMHP crystals.[41] Briefly, these models correlating blinking and trap depth/densities in QDs are not applicable to the perovskite nanocrystals. i.e. the mechanistic information we can currently obtain from the blinking behavior of perovskite nanocrystals, is only qualitatively. According to reported theories,[15, 41] ON and OFF state durations are related to the rate of switching between passive/active states of non-radiative (NR) centers in OMHP nanocrystals. In this work, a more frequent occurrence of longer ON states reflects a more stable passive state of the NR centers. We propose that chloride doping slows down the active trapping rate in fluctuating NR sites or decreases the number of NR centers. A similar phenomenon was also reported in OMHP nanocrystals by trap filling.[33, 37d] Trap density suppression due to trap filling by increasing the excitation power density results in more stable passive trap state and subsequent longer ON state durations. Therefore, we can imply a more stable passive state in this work. After chloride doping, the concentration of NR (deep trap) sites may be reduced resulting in bespoke stable passive state and subsequent longer and more frequent ON states. Regarding the similar distribution of OFF time durations, we speculate it may be related to the efficiency of charge trapping depending on the trap depth.[17] In other words, the mean OFF state times may be mainly dominated by some very efficient deep traps, finally resulting in almost the same OFF-state times in our study. Although the exact type of the very efficient traps cannot be determined, our work suggest that multi-defect passivation is key to obtain trap-free OMHP nanoparticles.

3. CONCLUSION

In this work, we demonstrate that advanced PL blinking studies of OMHP nanocrystals, are key to correctly assess the effect of Cl doping on defect types and densities. Here, $MAPbI_3$ NCs with the addition of 0%, 2%, and 5% of chloride were prepared and characterized structurally and optically. Despite the minute Cl doping, it plays a vital role in structure, morphology, and PL properties. When adding MACl to the precursor solution, the NCs end up to be more monocrystalline, slightly larger, and more plate-like. The PLQY of the Cl-doped NCs nearly doubled and also PL lifetime measurements resulted in almost doubled PL decay times. Next, the PL blinking behavior of the $MAPbI_3$, $MAPbI_3$-2%Cl and $MAPbI_3$-5%Cl NCs were studied comparatively for the first time. The ON distributions exhibited slightly higher power-law exponents (α increases from -1.33 to -1.11) with an increasing amount of chloride doping. All these findings indicate that, upon Cl doping, trap densities are reduced compared to pure $MAPbI_3$ NCs, suggesting that chloride efficiently passivates traps in $MAPbI_3$ NCs either by decreasing trap formation during the crystal growth or by inducing a shift of the trap states to a shallower level. These findings are useful for guiding defect passivation in a broad range of metal halide perovskite materials toward improving the performance of perovskite optoelectronic devices.

4. EXPERIMENTAL SECTION/METHODS

Nanocrystal synthesis and sample preparation

All the chemicals were used as received, including methylammonium iodide (MAI, 98%, Greatcell solar materials Pty Ltd.), Lead (II) iodide (PbI_2, 99%, Sigma-Aldrich), methylammonium chloride (MACl, 98%, Sigma-Aldrich), lead (II) chloride ($PbCl_2$, 98%, Sigma-Aldrich), trioctylphosphine oxide (TOPO, 99%, Aldrich), oleylamine (OAm, 70%, technical grade, Sigma-Aldrich), acetonitrile (ACN, 99.8%, Sigma-Aldrich), dimethyl sulfoxide (DMSO, ≥99.9%, ACS reagent), and toluene (ACS, Reag. Ph. Eur.).

Cl-doped perovskite NCs were produced by applying the injection-precipitation method. The precursor solution was prepared by dissolving PbI_2 (0.04 mmol, 18.8 mg) and MAI (0.12 mmol, 18.8 mg) in 20 mL of ACN. MACl (13.6 mg, 200 μmol) was dissolved in 1 ml DMSO. 0, 1, 2, 5, 9 and 11 molar% (Cl :I molar ratio) Cl-containing solutions were prepared by adding 0, 1, 2, 5, 8, 10 μl of the MACl solution, respectively, directly to 3 ml of the precursor solution. MACl was chosen as doping salt because MA-cation-related intrinsic defects do not contribute to mid-gap traps. In parallel, the capping agents, 72 μL of OAm and 60 mg of TOPO, were dissolved in 30 mL toluene as anti-solvent and divided into six batches under stirring. Five minutes after injection of 1.3 mL of the doped precursor solution to the vigorously stirred capping agent solutions, an extra 7 mL of toluene was added dropwise. The mixture was kept stirring at room temperature for 4 hours, resulting in a dark brown suspension containing $MAPbI_3$ nanocrystals. The dark brownish suspension was then washed twice by centrifugation for 30 minutes at 4200 rpm and the residue was re-dispersed in 4 mL of toluene. The final suspensions of $MAPbI_3$, $MAPbI_3$-1%Cl, $MAPbI_3$-2%Cl, $MAPbI_3$-5%Cl, $MAPbI_3$-9%Cl and $MAPbI_3$-11%Cl NCs were kept in the dark. Note that the total amount of Cl which was added to the precursor solution, did not necessarily all react to be incorporated into the $MAPbI_3$ NCs. To explore the effect of the DMSO solvent added while performing Cl-doping, additional samples comprising 0, 0.03, 0.07, 0.17, 0.27 and 0.33 volume% DMSO (DMSO : ACN volume ratio) were prepared by adding 0, 1, 2, 5, 8, 10 μl of DMSO solvent, respectively, into 3 mL of the $MAPbI_3$ precursor solution. The rest of the procedure remained the same as the one described above. SEM (scanning electron microscopy) and AFM (atomic force microscopy) were performed by respectively dropping 10 μl of the suspension onto a 5 mm × 5 mm silicon chip and mica substrate, which were dried at ambient conditions. For the wide-field microscope and time-resolved single-photon counting (TCSPC) measurements, 20 μl of the toluene suspension was dropped and spin-coated at 1500 rpm for 60 s onto a clean glass cover slide. Methylammonium lead chloride ($MAPbCl_3$) was prepared by mixing an equi-molar ratio of

MACl and $PbCl_2$ in DMSO (0.2 M), which was dropped on a clean silicon substrate and annealed at 160 ℃ for 10 minutes.

Characterization

Scanning Electron Microscope (SEM) images were obtained using a FEI Quanta FEG-250 environmental SEM equipped with a spectrometer for Energy-dispersive X-ray spectroscopy (EDS). X-ray diffraction (XRD) patterns were recorded on a Malvern PANalytical Empyrean diffractometer using a Debye-Scherrer transmission geometry equipped with a PIXcel3D solid-state detector using a Cu anode. X-ray photoelectron spectroscopy (XPS) was performed by a K-alpha Thermo spectrometer working with an Al K_α radiation at 1486.68 eV. Atomic Force Microscopy (AFM) images were acquired by a Smart-1000 (AIST-NT) and WSXM[42] software was used to determine particle thickness. The absorption spectrum was characterized by a Lambda 950 spectrophotometer. Steady-state photoluminescence spectra were measured on an Edinburgh FLS980 fluorimeter, with an excitation wavelength of 488 nm. The PL blinking time traces were recorded by an integrated optical and electron microscope system which consists of an FEI Quanta FEG-250 SEM equipped with an inverted optical microscope (Olympus IX71). The emission light is collected by an EM-CCD camera (Image-EM X2, Hamamatsu). All data were recorded over 3000 frames using a high-speed EM camera with an exposure time of 100 ms. A 488 nm laser was used as the excitation source. The PL blinking time trace was recorded by this integrated system, before capturing the SEM morphology images. PL time traces were extracted using a home-developed Igor super-resolution localization code. Half the intensity of the bright state, after subtracting the background, was used as the threshold to determine the ON/OFF times[27, 33, 37d]. Time-Correlated Single Photon Counting (TCSPC) data were recorded by a home-built confocal fluorescence lifetime imaging (FLIM) microscope. A pulsed 485 nm laser diode with a laser pulse frequency set at 2 MHz was used as the excitation source. The emission channel was filtered by a bandpass filter (705-755 nm).

Supporting Information

Supporting Information is available from the Wiley Online Library or from the author.

Acknowledgements

The authors acknowledge financial support from the Research Foundation - Flanders (FWO Grant Numbers S002019N, 1514220N, G.0B39.15, G.0B49.15, G.0962.13, G098319N, and ZW15_09-GOH6316), the Research Foundation - Flanders postdoctoral fellowships to J.A.S. and E.D. (FWO Grant Numbers 12Y7218N and 12O3719N, respectively), the KU Leuven Research Fund (C14/15/053 and C19/19/079), the Flemish government through long term structural funding Methusalem (CASAS2, Meth/15/04), the Hercules Foundation (HER/11/14), and the doctoral fellowship to H.J. from the China Scholarship Council (Grant number 201606220032). J.H. thanks the MPI for financial support as a MPI fellow.

Received: ((will be filled in by the editorial staff))
Revised: ((will be filled in by the editorial staff))
Published online: ((will be filled in by the editorial staff))

References

[1] J. Huang, Y. Shao, Q. Dong, The Journal of Physical Chemistry Letters 2015, 6, 3218.
[2] A. Kojima, K. Teshima, Y. Shirai, T. Miyasaka, Journal of the American Chemical Society 2009, 131, 6050.
[3] Best Research-Cell Efficiencies (NREL, https://www.nrel.gov/pv/assets/pdfs/best-research-cell-efficiencies.20200104.pdf.
[4] Y. Yang, J. You, Nature 2017, 544, 155.
[5] H. Jin, E. Debroye, M. Keshavarz, I. G. Scheblykin, M. B. Roeffaers, J. Hofkens, J. A. Steele, Materials Horizons 2019, 7, 397.
[6] I. G. Scheblykin, Advanced Energy Materials 2020, 2001724.
[7] a) G. Xing, N. Mathews, S. S. Lim, N. Yantara, X. Liu, D. Sabba, M. Grätzel, S. Mhaisalkar, T. C. Sum, Nature materials 2014, 13, 476; b) Y. Chen, H. Yi, X. Wu, R. Haroldson, Y. Gartstein, Y. Rodionov, K. Tikhonov, A. Zakhidov, X.-Y. Zhu, V. Podzorov, Nature communications 2016, 7, 12253.
[8] D. Meggiolaro, S. G. Motti, E. Mosconi, A. J. Barker, J. Ball, C. A. R. Perini, F. Deschler, A. Petrozza, F. De Angelis, Energy & Environmental Science 2018, 11, 702.
[9] a) M. Abdi-Jalebi, Z. Andaji-Garmaroudi, S. Cacovich, C. Stavrakas, B. Philippe, J. M. Richter, M. Alsari, E. P. Booker, E. M. Hutter, A. J. Pearson, Nature 2018, 555, 497; b) M. Saliba, T. Matsui, K. Domanski, J.-Y. Seo, A. Ummadisingu, S. M. Zakeeruddin, J.-P. Correa-Baena, W. R. Tress, A. Abate, A. Hagfeldt, Science 2016, 354, 206.
[10] G. Nan, X. Zhang, M. Abdi‐Jalebi, Z. Andaji‐Garmaroudi, S. D. Stranks, G. Lu, D. Beljonne, Advanced Energy Materials 2018, 8, 1702754.
[11] H. Min, M. Kim, S.-U. Lee, H. Kim, G. Kim, K. Choi, J. H. Lee, S. I. Seok, Science 2019, 366, 749.
[12] M. I. Saidaminov, J. Kim, A. Jain, R. Quintero-Bermudez, H. Tan, G. Long, F. Tan, A. Johnston, Y. Zhao, O. Voznyy, E. H. Sargent, Nature Energy 2018, 3, 648.
[13] T. Hwang, A. J. Yun, B. Lee, J. Kim, Y. Lee, B. Park, Journal of Applied Physics 2019, 126, 023101.

[14] M. Kuno, D. Fromm, H. Hamann, A. Gallagher, D. J. Nesbitt, The Journal of chemical physics 2001, 115, 1028.
[15] A. Merdasa, Y. Tian, R. Camacho, A. Dobrovolsky, E. Debroye, E. L. Unger, J. Hofkens, V. Sundström, I. G. Scheblykin, ACS nano 2017, 11, 5391.
[16] M. Gerhard, B. Louis, R. Camacho, A. Merdasa, J. Li, A. Kiligaridis, A. Dobrovolsky, J. Hofkens, I. G. Scheblykin, Nature communications 2019, 10, 1.
[17] H. Yuan, E. Debroye, E. Bladt, G. Lu, M. Keshavarz, K. P. Janssen, M. B. Roeffaers, S. Bals, E. H. Sargent, J. Hofkens, Advanced Materials 2018, 30, 1705494.
[18] S. T. Williams, F. Zuo, C.-C. Chueh, C.-Y. Liao, P.-W. Liang, A. K.-Y. Jen, ACS nano 2014, 8, 10640.
[19] Y. Tidhar, E. Edri, H. Weissman, D. Zohar, G. Hodes, D. Cahen, B. Rybtchinski, S. Kirmayer, Journal of the American Chemical Society 2014, 136, 13249.
[20] F. Xu, T. Zhang, G. Li, Y. Zhao, ChemSusChem 2017, 10, 2365.
[21] B. Conings, L. Baeten, C. De Dobbelaere, J. D'Haen, J. Manca, H. G. Boyen, Advanced Materials 2014, 26, 2041.
[22] M. Caputo, N. Cefarin, A. Radivo, N. Demitri, L. Gigli, J. R. Plaisier, M. Panighel, G. Di Santo, S. Moretti, A. Giglia, Scientific reports 2019, 9, 1.
[23] a) B. Philippe, B.-W. Park, R. Lindblad, J. Oscarsson, S. Ahmadi, E. M. Johansson, H. k. Rensmo, Chemistry of Materials 2015, 27, 1720; b) Y. Luo, S. Gamliel, S. Nijem, S. Aharon, M. Holt, B. Stripe, V. Rose, M. I. Bertoni, L. Etgar, D. P. Fenning, Chemistry of Materials 2016, 28, 6536.
[24] C. Mu, J. Pan, S. Feng, Q. Li, D. Xu, Advanced Energy Materials 2017, 7, 1601297.
[25] V. L. Pool, A. Gold-Parker, M. D. McGehee, M. F. Toney, Chemistry of Materials 2015, 27, 7240.
[26] O. Vybornyi, S. Yakunin, M. V. Kovalenko, Nanoscale 2016, 8, 6278.
[27] B. Rogez, H. Yang, E. Le Moal, S. Lévêque-Fort, E. Boer-Duchemin, F. Yao, Y.-H. Lee, Y. Zhang, K. D. Wegner, N. Hildebrandt, A. Mayne, G. Dujardin, The Journal of Physical Chemistry C 2014, 118, 18445.
[28] E. Mosconi, D. Meggiolaro, H. J. Snaith, S. D. Stranks, F. De Angelis, Energy & Environmental Science 2016, 9, 3180.
[29] D.-Y. Son, J.-W. Lee, Y. J. Choi, I.-H. Jang, S. Lee, P. J. Yoo, H. Shin, N. Ahn, M. Choi, D. Kim, N.-G. Park, Nature Energy 2016, 1, 1.
[30] M. Jung, T. J. Shin, J. Seo, G. Kim, S. I. Seok, Energy & Environmental Science 2018, 11, 2188.
[31] Y. Liu, H. Lu, J. Niu, H. Zhang, S. Lou, C. Gao, Y. Zhan, X. Zhang, Q. Jin, L. Zheng, AIP Advances 2018, 8, 095108.
[32] a) T. Ando, S. P. Bhamidimarri, N. Brending, H. Colin-York, L. Collinson, N. De Jonge, P. De Pablo, E. Debroye, C. Eggeling, C. Franck, Journal of physics D: Applied physics 2018, 51, 443001; b) E. Debroye, J. Van Loon, X. Gu, T. Franklin, J. Hofkens, K. P. Janssen, M. B. Roeffaers, Particle & Particle Systems Characterization 2016, 33, 412.
[33] Y. Tian, A. Merdasa, M. Peter, M. Abdellah, K. Zheng, C. S. Ponseca Jr, T. n. Pullerits, A. Yartsev, V. Sundström, I. G. Scheblykin, Nano letters 2015, 15, 1603.
[34] G. Yuan, C. Ritchie, M. Ritter, S. Murphy, D. E. Gómez, P. Mulvaney, The Journal of Physical Chemistry C 2017, 122, 13407.
[35] H. Yuan, E. Debroye, K. Janssen, H. Naiki, C. Steuwe, G. Lu, M. l. Moris, E. Orgiu, H. Uji-i, F. De Schryver, The Journal of Physical Chemistry Letters 2016, 7, 561.
[36] J. N. Clifford, T. D. Bell, P. Tinnefeld, M. Heilemann, S. M. Melnikov, J.-i. Hotta, M. Sliwa, P. Dedecker, M. Sauer, J. Hofkens, The Journal of Physical Chemistry B 2007, 111, 6987.
[37] a) Y. J. Bae, N. A. Gibson, T. X. Ding, A. P. Alivisatos, S. R. Leone, The Journal of Physical Chemistry C 2016, 120, 29484; b) X. Wen, A. Ho-Baillie, S. Huang, R. Sheng, S.

Chen, H.-c. Ko, M. A. Green, Nano Letters 2015, 15, 4644; c) A. Mukherjee, K. K. Ray, C. Phadnis, A. Layek, S. Bera, A. Chowdhury, The Journal of Chemical Physics 2019, 151, 084701; d) H. Yuan, E. Debroye, G. Caliandro, K. P. Janssen, J. Van Loon, C. E. Kirschhock, J. A. Martens, J. Hofkens, M. B. Roeffaers, ACS omega 2016, 1, 148.
[38] B. Chen, P. N. Rudd, S. Yang, Y. Yuan, J. Huang, Chemical Society Reviews 2019, 48, 3842.
[39] H. Tan, A. Jain, O. Voznyy, X. Lan, F. P. G. De Arquer, J. Z. Fan, R. Quintero-Bermudez, M. Yuan, B. Zhang, Y. Zhao, Science 2017, 355, 722.
[40] M. Kuno, D. Fromm, S. Johnson, A. Gallagher, D. J. Nesbitt, Physical Review B 2003, 67, 125304.
[41] I. Y. Eremchev, A. O. Tarasevich, J. Li, A. V. Naumov, I. G. Scheblykin, Advanced Optical Materials 2020, 2001596.
[42] I. Horcas, R. Fernández, J. Gomez-Rodriguez, J. Colchero, J. Gómez-Herrero, A. Baro, Review of scientific instruments 2007, 78, 013705.

Direct Experimental Evidence of Chloride-Induced Trap Passivation in Lead Halide Perovskites

Handong Jin, Julian A. Steele, Ruolin Cheng, Nagma Parveen, Maarten B. J. Roeffaers, Johan Hofkens and Elke Debroye**

TOC figure